Batteries & Supercaps

Research Article
doi.org/10.1002/batt.202400506

Chemistry Europe
European Chemical Societies Publishing

www.batteries-supercaps.org

Life After Death: Re-Purposing End-of-Life Supercapacitors for Electrochemical Water Desalination

Panyu Ren,[a, b] Mohammad Torkamanzadeh,[a] Stefanie Arnold,[a] Emmanuel Pameté,[a] and Volker Presser*[a, b, c]

This study explores the potential of re-purposing end-of-life commercial supercapacitors as electrochemical desalination cells, aligning with circular economy principles. A commercial 500-Farad supercapacitor was disassembled, and its carbon electrodes underwent various degrees of modification. The most straightforward modification involved NaOH-etching of the aluminum current collector to produce free-standing carbon films. More advanced modifications included CO_2 activation and binder-added wet processing of the electrodes. When evaluated as electrodes for electrochemical desalination via capacitive deionization of low-salinity (20 mM) NaCl solutions, the minimally modified NaOH-etched carbon electrodes achieved an average desalination capacity of 5.8 mg g^{-1} and a charge efficiency of 80 %. In contrast, the CO_2-activated, wet-processed electrodes demonstrated an improved desalination capacity of 7.9 mg g^{-1} and a charge efficiency above 90 % with stable performance over 20 cycles. These findings highlight the feasibility and effectiveness of recycling supercapacitors for sustainable water desalination applications, offering a promising avenue for resource recovery and re-purposing in pursuing environmental sustainability.

Introduction

We have seen a significant shift towards a circular economy emphasizing sustainability and waste reduction in recent years.[1] This transition aims to minimize waste and maximize the lifecycle of products, fostering a more sustainable approach to resource management. As a result, innovative strategies for the intelligent re-purposing of spent resources have garnered significant academic and industrial interest. Numerous studies now explore these strategies, seeking to develop efficient methods to transform waste into valuable inputs for new products and processes, contributing to a more sustainable future. Examples include carbon materials derived from a host of bio-wastes[2,3] or manufactured wastes such as cigarette filters[4–6] and face masks during the pandemic,[7] utilized as electrodes for energy storage devices or electrochemical desalination systems. Non-carbon waste has also been the subject of many other studies, such as re-using rusted iron wire waste collected from construction sites as supercapacitor electrodes made of carbon/Fe_3O_4 nanocomposites.[8]

In addition to the derivatization of wastes, direct re-use of end-of-life devices is another promising approach toward a circular economy. Examples include disassembling old electrical motors and directly re-using the permanent magnets in their core, containing rare earth elements, in a new motor.[9] The direct re-use strategy is widely applied for the recovery of magnets.[10,11] For batteries, it depends on the state of health and target application conditions. For example, batteries from retired electric vehicles can often be re-purposed for a second-life application without dismantling the devices for stationary applications. Also, recent research explores the regeneration of spent battery electrodes rather than the elaborate process of elemental recovery through hydrometallurgical or pyrometallurgical processing.[12,13] Recently, we also reported a facile recycling process for end-of-life MXene ($Ti_3C_2T_x$) electrodes for re-use in Li-ion and Na-ion battery anodes.[14] Most commonly, emerging on a large scale due to evolving governmental regulations,[15,16] most batteries at present and in the near future will undergo a complete recycling process, much like recycling glass or paper toward closing the loop for precious element recovery toward new cell production.

As a technology different from batteries, supercapacitors enable rapid and effective energy storage for high-power applications ranging from consumer electronics to renewable energies.[17,18] Due to their high-power capabilities, supercapacitors are coupled with batteries in almost any battery-powered system to either render burst-mode delivery of electric energy, such as in a camera flash, or to store a suddenly generated high amount of electric energy, such as in regenerative braking.[19] Depending on the operational conditions, commonly, after hundreds of thousands of cycles,[20,21] the supercapacitors reach their end of life, which is characterized by a decrease in their

[a] P. Ren, M. Torkamanzadeh, S. Arnold, E. Pameté, V. Presser
INM – Leibniz Institute for New Materials, D2 2, 66123 Saarbrücken, Germany
E-mail: volker.presser@leibniz-inm.de

[b] P. Ren, V. Presser
Department of Materials Science & Engineering, Saarland University, Campus D2 2, 66123 Saarbrücken, Germany

[c] V. Presser
saarene, Saarland Center for Energy Materials and Sustainability, Campus C4 2, 66123 Saarbrücken, Germany

Supporting information for this article is available on the WWW under https://doi.org/10.1002/batt.202400506

capacitance (−20%) and/or increase in their equivalent series resistance (+100%).[22,23] Without containing precious elements, such as lithium, cobalt, or nickel, supercapacitor recycling, while eco-relevant, faces particular economic challenges.[24] Although various re-use or recycling strategies[25,26] such as shredding,[27] thermal treatments,[28,29] and hydrometallurgical processes[30] have been so far developed for lithium-ion battery recycling, supercapacitor recycling[31] has not seen significant attention to date. End-of-life supercapacitor devices are, as a result, not effectively recycled. Conventional supercapacitors may not contain precious materials like batteries, but there may be potentially hazardous electrolytes (e.g., acetonitrile and $TEABF_4$) dispersed in the activated carbon electrodes.[32] Hence, re-using activated carbon can partially compensate for the cost of recycling. It was reported that a method of supercapacitor recycling based on shredding and mild thermal treatment can recycle activated carbon, aluminum, and acetonitrile while leaving the electrolyte salt and the polymer binder behind in the activated carbon, making the recycled activated carbon has a high surface area up to 1200 $m^2 g^{-1}$ and 40 mass% of acetonitrile with high purity.[31] Chodankar et al. regenerated activated carbon materials from end-of-life supercapacitors through a straightforward thermal activation process and successfully reintegrated them into high-voltage, ultra-stable supercapacitors.[33] Additionally, Wu et al. successfully recycled activated carbon (surface area up to 1403 $m^2 g^{-1}$) from a used HYPSC-002R7–3000 supercapacitor and re-purposed it as a cost-effective adsorbent for the efficient removal of toxic Ag(I) and Cr(VI) ions from aqueous solutions.[34] This approach is not just recycling the used supercapacitor material for the same purpose but adapting it for the treatment of contaminated wastewater. Among various water treatment techniques, capacitive deionization is regarded as the most effective process for ion separation due to its low cost, high efficiency, and ease of operation.[35] Various electrochemical desalination strategies have been developed in different water media,[35] which included desalination,[36,37] water softening,[38,39] and heavy metal removal.[40–43] Developing a simple, cost-effective method for recycling supercapacitors demands significant research attention, particularly regarding the potential hazards posed by conventional electrolytes, solvents, and polymer binders at the end of the device's life. Additionally, the re-use of recycled materials should be considered.[32]

As the first study of this type, the present work examines the feasibility of turning a commercial supercapacitor with a capacitance of 500 F into an electrochemical desalination cell for capacitive deionization. To transform its application, we investigate several routes, ranging from the least to the highest modification degrees made to the device. The least-invasive modification degree pertains to making holes in the supercapacitor device and passing a saline aqueous electrolyte (NaCl) through it. The highest modification degree pertains to a whole disassembly of the supercapacitor, removal of its carbon electrodes (separating the aluminum substrate and activated carbon electrodes by NaOH etching), reprocessing them into new electrodes, and testing them as electrodes for electrochemical desalination. The electrode fabrication in the latter route also branches out into CO_2 activation and binder-added wet processing of the electrodes (Figure 1). The CO_2 activation is conducted with the goal of potential enhancement in the porosity and wettability of the electrodes. We then assess the merit of each of the said routes in terms of desalination capacity, charge efficiency, and cycle stability, together with the efforts associated with each trajectory.

Results and Discussion

Physicochemical Characterizations

Figure 1 schematically shows the procedure through which the commercial supercapacitor electrodes were reprocessed and re-purposed for use as electrochemical desalination electrodes. Photographs and videos from the disassembly process are in *Supporting Information*, Figure S1 and Video S1–2. The obtained electrode coating from the commercial supercapacitor has been subjected to detailed physicochemical characterizations. To remove the aluminum current collector from the carbon electrodes, the electrode bundle was immersed into a 10 mass% aqueous NaOH solution. The scanning electron

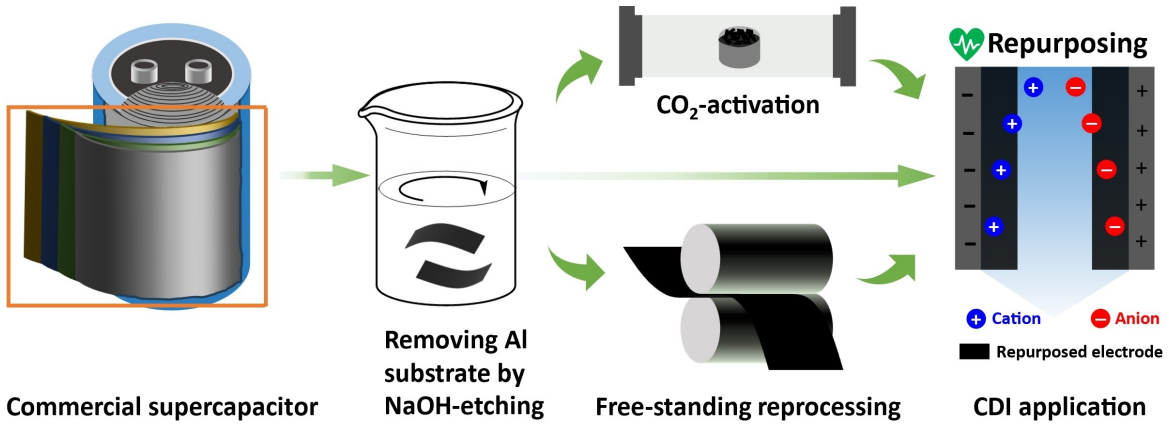

Figure 1. Schematic representation of the step-by-step processes involved in disassembling the commercial supercapacitor in this study and their re-purposing for electrochemical desalination electrodes.

Research Article
doi.org/10.1002/batt.202400506
Chemistry Europe
European Chemical Societies Publishing

micrographs in Figure 2A–B show the electrode films after being detached from the aluminum current collector and thoroughly dried under vacuum. The etching process could cause the cracked features on the electrode. However, the electrode delivers a homogenous and dense packing of carbon particles with an average size of around 2 μm. Scanning electron micrographs of the supercapacitor separator and additional images of the supercapacitor electrodes are provided in *Supporting Information*, Figure S2–S3. The relatively large particles (Figure 2A–B and *Supporting Information*, Figure S3) are attributed to activated carbon used in the electrode surrounded by small debris (assumed to be carbon black particles used as a conductive additive).

The X-ray diffraction (XRD) data in Figure 2C shows broad reflections at around 23° and 43° 2θ in alignment with incompletely graphitic carbon (PDF# 41-1487). The sharp reflection at 18° 2θ indicates the presence of a polymer binder, such as polytetrafluoroethylene (PTFE), to hold the active

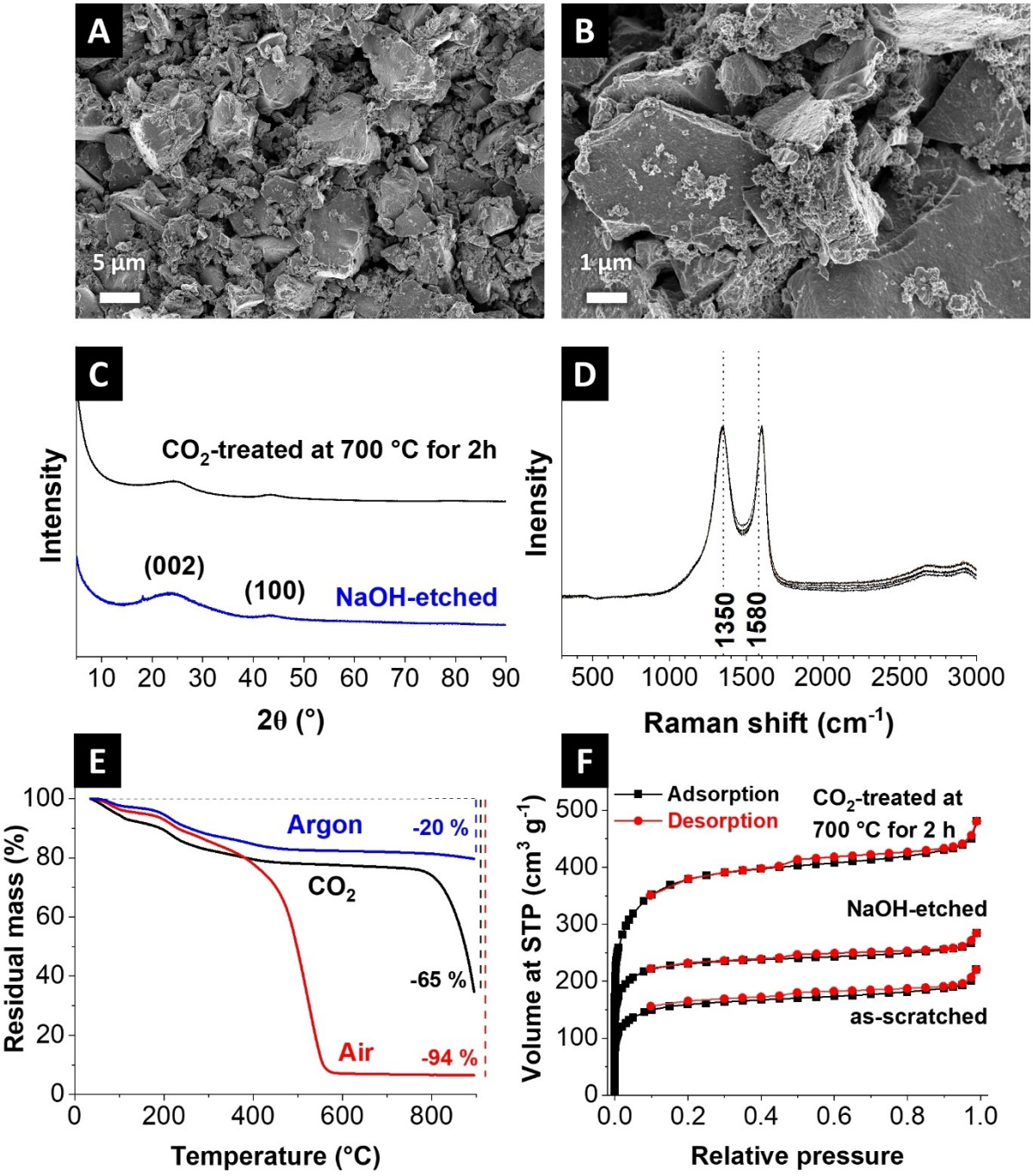

Figure 2. (A, B) Scanning electron micrographs of NaOH-etched carbon electrode peeled off from the aluminum current collector, its (C) X-ray diffraction pattern (including pattern after CO_2 activation at 700 °C for 2 h), (D) Raman spectra, (E) thermogravimetric analysis in argon, air, and CO_2 atmospheres, and (F) nitrogen gas sorption measurement at −196 °C. (STP: standard temperature and pressure).

materials together and enhance their adhesion to the current collector (aluminum foil). The X-ray diffractogram of the CO_2-activated sample (700 °C for 2 h) shows no significant difference from the etched sample, and the prevalence of broad peaks aligns with the presence of incompletely crystalline/amorphous lattices. The thermal CO_2 treatment did not produce a crystalline structure, and the reflection of the binder material is no longer present due to decomposition during the heat treatment.

Elemental analysis (Table 1) of the supercapacitor electrodes (labeled NaOH-etched) reveals a 68 mass% carbon content and a relatively large oxygen content of 23 ± 3 mass%, possibly arising from the partial oxidation during NaOH etching. The fluorine content of around 1 mass% documents the presence of standard polymeric binders such as polytetrafluoroethylene or polyvinylidene fluoride.

Raman spectra (Figure 2D) show the characteristic D-mode, G-mode, and D'-mode at 1350 cm^{-1}, 1580 cm^{-1}, and 2680 cm^{-1}, respectively. The G-mode corresponds to graphitic carbon in-plane vibrations with E_{2g} symmetry, and the D-mode is generally associated with breathing vibrations of sp^2 rings, characterizing A_{1g} symmetry disallowed in graphite, further confirming that the commercial supercapacitor consisted of carbon as the active material.[44,45]

Thermogravimetric analysis (TGA) revealed that the supercapacitor electrode experiences complete mass loss in air at temperatures above 500 °C, while under an argon atmosphere, only 20% of the initial mass is lost when heated up to 800 °C (Figure 2E). The significant mass loss in the air indicates that the electrode material undergoes combustion (oxidation) processes at high temperatures. The lower decomposition temperature than other carbonaceous materials suggests a larger surface area and/or smaller particle sizes.[46,47] The remaining 6% of the sample's mass is likely due to residues from the aluminum current collector (as confirmed by EDX analysis in Table 1), potentially in Al_2O_3, which might form during NaOH etching of the black mass. Under an inert argon atmosphere, the 22% mass loss indicates a lower reactivity, representing the extent of degradation and/or oxidation processes in the absence of oxygen at temperatures up to 800 °C. To better understand the behavior of the electrode under CO_2 activation, samples were also tested in a CO_2 atmosphere. Besides the initial footprint of the binder decomposition, 76 mass% of the sample remains up to the temperature of 750 °C. At around 900 °C, the residual mass amounts to 65%, indicating only a partial combustion/oxidation under a CO_2 environment.

To study the pore size characteristics of the pristine supercapacitor electrode, we gently scratched the surface of the carbon-coated aluminum current collector to collect the carbon powder. Nitrogen gas sorption measurements were performed on the latter material (as-scratched) and the NaOH-etched supercapacitor electrode (Figure 2F). The nitrogen adsorption-desorption results show isotherm shapes typical for microporous carbons.[48] The analysis shows specific surface areas of 520 $m^2 g^{-1}$ (average pore size of 0.57 nm) and 810 $m^2 g^{-1}$ (average pore size of 0.61 nm) for the as-scratched and NaOH-etched materials, respectively, showing increases in pore volume after the NaOH etching (Table 2). To study potential enhancement in the electrochemical desalination performance, we also performed CO_2 treatment on the supercapacitor electrodes to modify pore size characteristics (*Supporting Information*, Figure S4). Conducted at 700 °C for 2 h, the CO_2 treatment of the supercapacitor electrodes significantly increased the specific surface area to 1216 $m^2 g^{-1}$ and the average pore size to 0.79 nm, even though the morphology showed no visible change (*Supporting Information*, Figure S3). Our further experimentations for physical activation by adjusting the maximum holding temperature and duration did not result in substantially higher surface areas (*Supporting Information*, Table S1, and Figure S5).

Table 1. Elemental analysis of the NaOH-etched carbon electrode, removed from the aluminum substrate.

Element	EDX (mass%)	CHNS–O (mass%)
C	84 ± 18	67.9 ± 0.5
H	–	3.4 ± 0.1
N	–	2.5 ± 2.5
S	–	–
O	12 ± 14	23 ± 3
F	2 ± 1	–
Al	2 ± 4	–
Na, Si, Br	< 1	–

Electrochemical Characterization of the Recycled Electrodes

The analysis of the as-extracted carbon electrode from the commercial supercapacitor (NaOH-etched) in a 1 M aqueous NaCl solution by cyclic voltammetry towards hydrogen evolution is shown in Figure 3A. Initially, as the negative vertex

Table 2. Summary of gas sorption analysis performed on the as-scratched supercapacitor electrode, after NaOH etching, and after the subsequent CO_2 treatment (QSDFT: quenched solid density functional theory, BET: Brunauer-Emmett-Teller theory).

Sample	Surface area QSDFT ($m^2 g^{-1}$)	Surface area BET ($m^2 g^{-1}$)	Average pore width d_{50} (nm)	Pore volume ($cm^3 g^{-1}$)
As-scratched	520	517	0.57	0.28
NaOH-etched	810	889	0.61	0.37
CO_2-treated at 700 °C for 2 h	1216	975	0.79	0.64

Research Article
doi.org/10.1002/batt.202400506
Chemistry Europe
European Chemical Societies Publishing

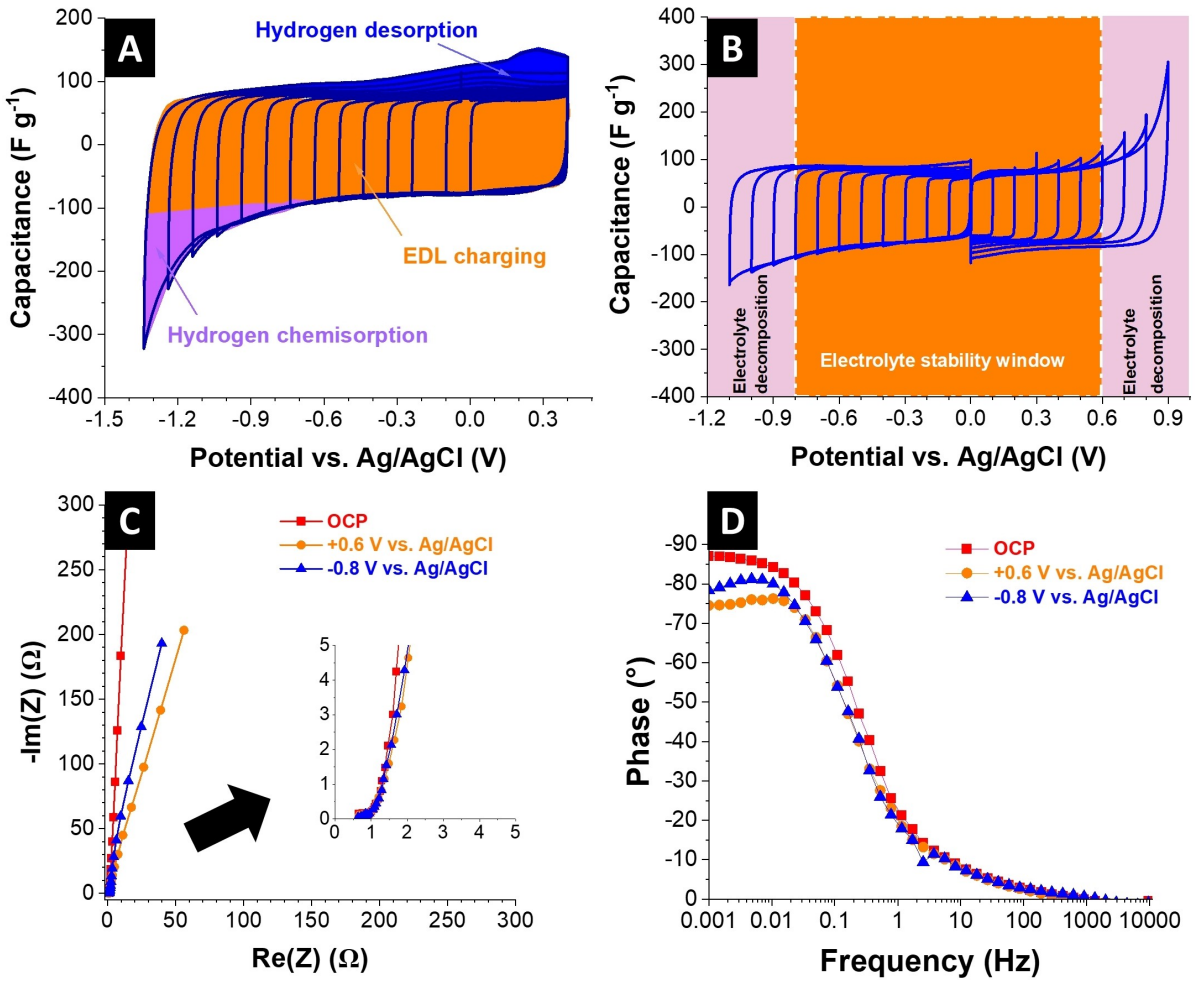

Figure 3. Half-cell electrochemical characterizations of NaOH-etched supercapacitor electrodes in 1 M aqueous NaCl solutions, including (A) the analysis of the voltammograms at negative polarization and (B) cycling voltammetry at negative and positive polarizations; (C) Nyquist plots of the impedance spectra and (D) Bode diagrams at various potentials (OCP: open circuit potential).

potential is reduced, the cyclic voltammograms demonstrate a characteristic pattern associated with electrical double-layer (EDL) charging. This phenomenon persists until the electrode reaches a potential of −0.7 V vs. Ag/AgCl. However, electrochemical water reduction occurs with a further decrease in the vertex potential, leading to the generation of nascent hydrogen. This hydrogen is produced and chemisorbed onto the carbon electrode.[49] As the vertex potential dips below −0.7 V vs. Ag/AgCl, a redox peak appears at around +0.15 V vs. Ag/AgCl during the anodic scan, suggesting the desorption of the previously chemisorbed hydrogen. When pushing the vertex potential further down to −1.3 V vs. Ag/AgCl, the negative current leap due to hydrogen chemisorption and the desorption counterpart during the anodic scan are more intense. This observation aligns with previous work demonstrating that applying a low potential to a porous carbon electrode in an aqueous environment triggered the creation and adsorption of nascent hydrogen on the carbon surface accompanied by hydroxyl OH^- ions.[50] This chemical environment led to localized changes in pH within the porosity and a negative shift in the Nernst potential.[49,50]

Accordingly, to assess the electrochemical stability region of the electrolyte, cyclic voltammograms were recorded separately on freshly extracted (NaOH-etched) electrodes, with both negative and positive polarizations (Figure 3B). During the negative sweeps, the negative vertex potential was gradually decreased from 0.0 V vs. Ag/AgCl in increments of 0.1 V. In contrast, during the positive sweeps, the positive vertex potential was gradually increased from 0.0 V vs. Ag/AgCl by the same increments.[51] This process continued until the electrolyte decomposition was observed in both cells. The region of electrolyte stability, characterized by purely box-like shapes of the cyclic voltammograms representing the EDL charging, was found between −0.8 V vs. Ag/AgCl and +0.6 V vs. Ag/AgCl by calculating the S-values for the negative and negative polarizations (*Supporting Information*, Figure S6).

The negatively polarized electrode's potential limit is −0.8 V vs. Ag/AgCl, which is lower than the thermodynamic reduction potential of water at the measured electrolyte pH of 5.6 (E_H = −0.527 V vs. Ag/AgCl). This indicates that when our NaOH-etched supercapacitor electrode is polarized below the hydrogen evolution potential in a 1 M aqueous NaCl solution, the

OH^- anions produced by water electrolysis are trapped in the carbon's pores.[49] This results in a local pH increase and a negative shift in the Nernst hydrogen evolution potential by 0.27 V. Conversely, below −0.8 V vs. Ag/AgCl cyclic voltammograms displaying nascent parasitic shapes indicated electrolyte decomposition.[50] Cyclic voltammograms of the CO_2-activated electrodes show similar stability regions (*Supporting Information*, Figure S7).

In addition to the cyclic voltammetry results, we also examined electrochemical impedance spectroscopy (EIS) data from the same experimental conditions to comprehensively understand the electrochemical performance. The EIS measurements in Figure 3C–D were conducted at three distinct electrode potentials: open circuit potential (OCP), −0.8 V vs. Ag/AgCl, and +0.6 V vs. Ag/AgCl. At OCP (Figure 3C), the equivalent series resistance (ESR) was determined to be 0.50 Ωcm^2, closely mirrored by the ESR values of 0.49 Ωcm^2 at −0.8 V vs. Ag/AgCl and 0.51 Ωcm^2 at +0.6 V vs. Ag/AgCl.

The phase angle versus frequency plots (Figure 3D) provide insights into the system's impedance behavior. At OCP, a phase angle of 87° was observed, indicative of a highly capacitive response. At −0.8 V vs. Ag/AgCl, the phase angle slightly decreased to 78°, suggesting a subtle shift towards a more resistive behavior. Finally, at 0.6 V vs. Ag/AgCl, the phase angle further decreased to 75°, signifying a shift towards even greater resistive behavior.

A fresh commercial supercapacitor with the same type as the one disassembled above underwent long-term electrochemical characterization. The specifications of the commercial supercapacitor provided by the manufacturer are listed in *Supporting Information*, Table S2. After soldering cables to the supercapacitor terminals (*Supporting Information*, Figure S8), the cylindrical cell was subjected to charging and discharging cycles by applying an external current of 1 A for over 11,000 cycles. The obtained cell voltage versus time plots and cycle stability tests are shown in *Supporting Information*, Figure S9. Despite operating at a relatively low current intensity of 1 A, given that the present supercapacitor can nominally be charged at a maximum of 230 A, the cell only achieves a capacitance of approximately 0.5 F (compared to 500 F as per manufacturer specifications).

Electrochemical Desalination with the Recycled Electrodes

As a first step to re-purposing and re-using the supercapacitor electrodes, holes were drilled in the two ends of the cylindrical supercapacitor, which allows direct flow of the aqueous solution (20 mM NaCl) through the cell (*Supporting Information*, Figure S10). No significant effluent water conductivity (concentration) reduction was observed upon charging the cell. The latter could be due to the electro-oxidation of aluminum current collectors upon their contact with aqueous NaCl electrolyte. As such, separate electrochemical water desalination cells were made with the electrodes extracted from another fresh supercapacitor cell.

We conducted a series of tests on the newly assembled cells to further investigate and validate the feasibility of using repurposed supercapacitor electrodes for desalination. Figure 4A shows the concentration change profiles of the effluent stream of a symmetric electrochemical desalination cell with NaOH-etched supercapacitor electrodes cycled in 20 mM NaCl electrolyte. Distinct decrease and rise concentration patterns were observed upon cycling the cell by charging at 1.2 V and discharging at 0.3 V, respectively. The mechanical properties of the electrodes were insufficient because we directly repurposed the thin electrode sheets after NaOH etching as electrodes for the desalination application. The analysis of the electrochemical desalination performance during 20 cycles (Figure 4B) yields an average desalination capacity (DC) of 5.8 mg g^{-1} and charge efficiency (CE) above 80%. We have previously shown that predictive tools based on the modified Donnan model could link the pore structure of porous carbon electrodes to their desalination performance.[52,53] Feeding the latter model with the pore size distributions of the NaOH-etched electrode (*Supporting Information*, Figure S4A) results in a DC of 6.4 mg g^{-1}, assuming a CE of 100%.

To enhance the DC as well as the flexibility of the electrodes, we have reprocessed the latter electrodes through the wet processing approach by admixing 5 mass% PTFE binder to them and calendaring it to form uniform, free-standing electrodes with a thickness of 600 μm. As presented in Figure 4C–D, the reprocessed electrode, however, showed lower DC values (3.8 mg g^{-1}). The latter could be due to the pore blockage in the carbon electrodes caused by adding the polymeric binder and increased electrode thickness. We then performed a series of heat treatments on the NaOH-etched supercapacitor electrodes in a CO_2 environment to activate the carbon electrodes (*Supporting Information*, Table S1), followed by admixing 5 mass% binder and calendaring. The CO_2 activation at 700 °C for 2 h has improved electrochemical desalination performance metrics (Figure 4E–F) compared to NaOH-etched electrodes (Figure 4A–B) and the CO_2-activated electrode at 800 °C for 1 h (*Supporting Information*, Figure S11). Namely, a DC of 7.9 mg g^{-1} and a CE of above 90% was achieved for the CO_2-treated electrodes and a more stable performance throughout 20 cycles. Given the pore size distribution of the CO_2-activated carbon material (*Supporting Information*, Figure S4B), an estimated DC of 8.7 mg g^{-1} is obtained, assuming a CE of unity using the predictive model outlined above.[52,53] The latter enhancement in NaCl removal capacity and stability of carbon electrodes upon CO_2 activation agrees with previous reports.[54,55] It is attributed to a better wettability of the CO_2-activated electrodes,[55] their higher surface area, larger pore volume (Table 2), and a possible de-blocking of the supercapacitor carbon pores, which were previously immersed in an organic electrolyte.[56]

The Kim-Yoon plot,[57] analogous to the Ragone plot in the energy storage field, is a tool for assessing performance metrics in electrochemical desalination by mapping desalination capacity against rate. As illustrated in Figure 5, while reprocessing (admixing 5 mass% binder) of the recovered supercapacitor electrode negatively impacts the DC, it slightly improves its

Research Article
doi.org/10.1002/batt.202400506
Chemistry Europe
European Chemical Societies Publishing

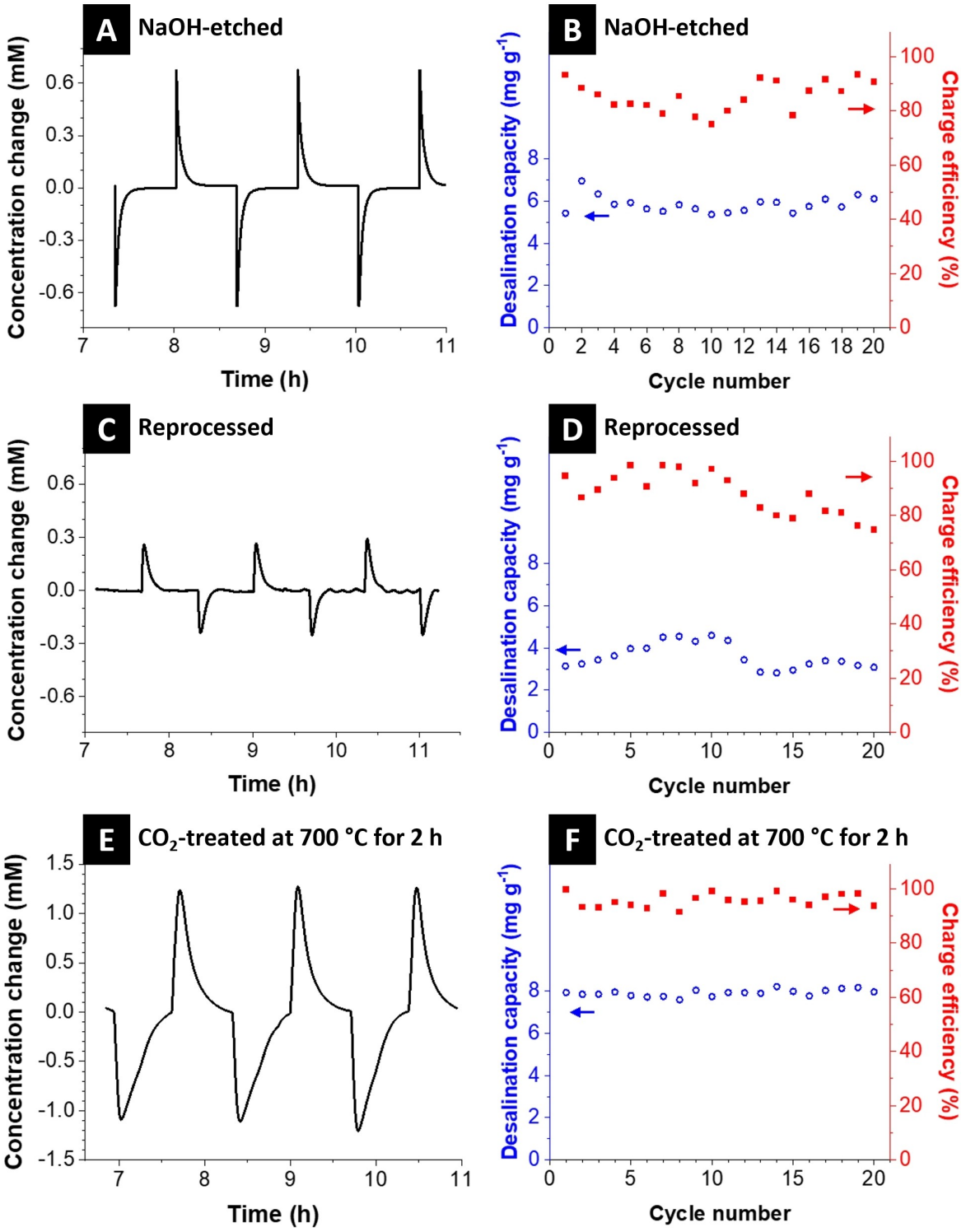

Figure 4. NaCl concentration-time profiles of the effluent water of the electrochemical cells made from the (A) NaOH-etched supercapacitor electrodes, (C) reprocessed electrodes, and (E) CO_2-treated electrodes at 700 °C for 2 h; Desalination capacity and charge efficiencies of the (B) NaOH-etched supercapacitor electrodes, (D) reprocessed electrodes, and (F) CO_2-treated and reprocessed electrodes at 700 °C for 2 h.

maximum salt removal rate from 0.007 mg g^{-1} s^{-1} (for NaOH etched electrode) to 0.008 mg g^{-1} s^{-1} (reprocessed electrode). The latter desalination rates are generally lower than commercial activated carbon (YP-80 F, Kuraray) film electrodes (~0.011 mg g^{-1} s^{-1}) when tested under conditions like electrodes for electrochemical desalination of aqueous 20 mM NaCl.[58] The relatively lower desalination rates in the present work could be explained by the sub-nanometer pore regimes of the supercapacitor carbon electrodes, which are in the range of 0.6–0.8 nm (Table 2), compared to the larger pore sizes (~1.4 nm) of

Research Article
doi.org/10.1002/batt.202400506
Chemistry Europe
European Chemical Societies Publishing

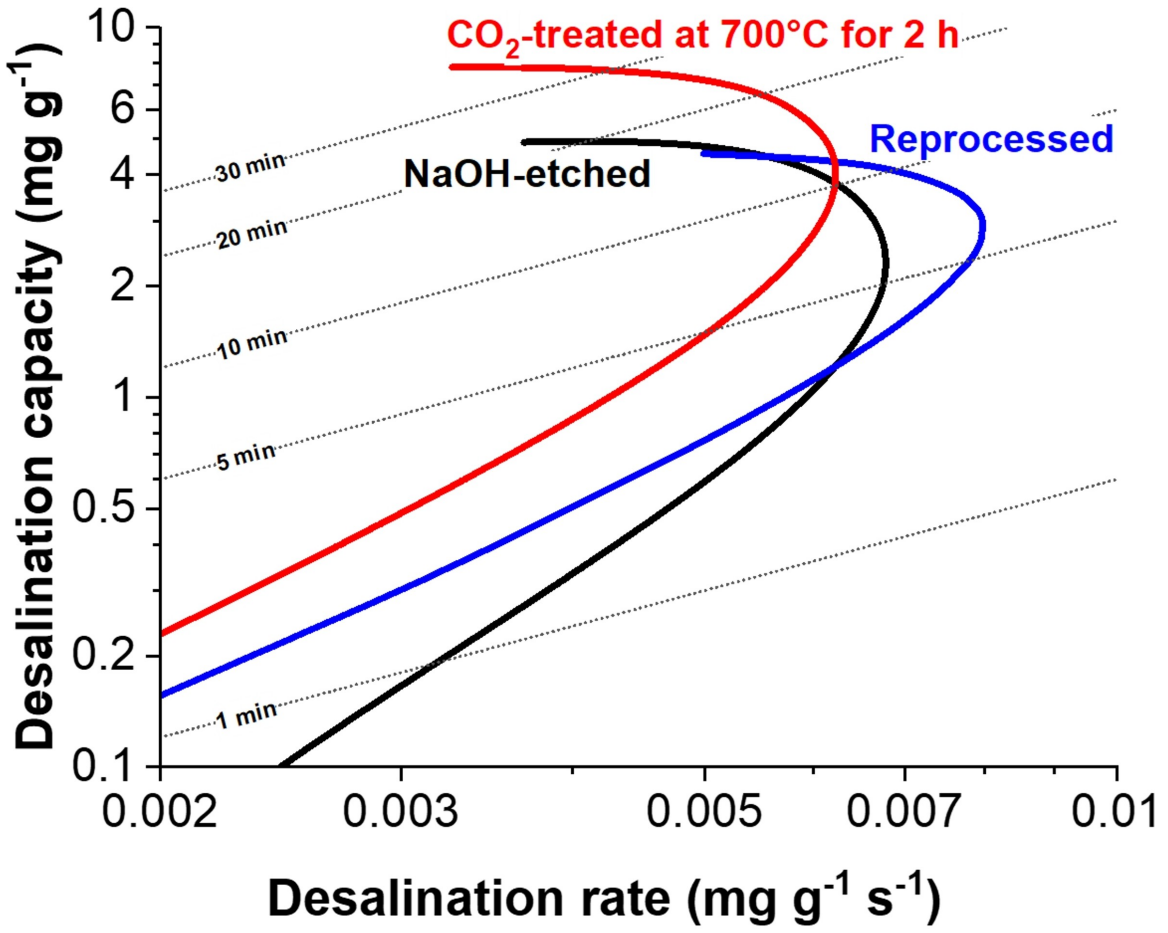

Figure 5. Electrochemical performance of NaOH-etched supercapacitor electrodes, reprocessed electrodes, and CO_2-treated at 700 °C for 2 h electrodes regarding desalination capacity and rates (Kim-Yoon plot).

carbon films in our previous work.[58] However, the CO_2 activation and reprocessing significantly improve the DC while having minimal influence on the desalination rate. Additionally, we evaluated the energy consumption of the electrodes used, as shown in Table 3. The CO_2-treated electrodes provide the best desalination performance and overall lower energy consumption (41.5 Wh mol^{-1}).

Although there is a rich literature on electrochemical desalination with carbon electrodes derived from the pyrolysis of a host of biomass sources,[59–62] there are no reports to the best of our knowledge on recycling or re-purposing an already-existing electrode material for electrochemical desalination. Nevertheless, a comparison is made to adjacent works to provide a broader context for the present study (as listed in *Supporting Information*, Table S3). While carbon from commercial sources typically yields desalination capacities of 10–16 mg g^{-1}, the derived carbons from waste sources vary mainly depending on their source, pyrolysis, and activation routes. This comparison underscores our approach's novelty and potential impact, paving the way for future research to explore and refine the re-purposing of supercapacitor materials for sustainable desalination technologies. CO_2 activation enhances the electrochemical desalination performance, which indicates that the current performance metrics can be significantly improved with further fine-tuning of the activation parameters. Further optimizing the CO_2 activation process could yield more developed carbons with enhanced properties.[63]

Table 3. Energy consumption of supercapacitor electrode after NaOH etching, reprocessed, and after the subsequent CO_2 treatment.

Sample	Energy consumption (Wh mol^{-1})
NaOH-etched	60.7
Reprocessed	42.6
CO_2-treated at 700 °C for 2 h	41.5

A Look at the Market and Volume of Activated Carbon Supercapacitors

The global supercapacitor market, valued at approximately 4.5 billion USD in 2023, is poised for substantial growth projected to exceed 12 billion USD by 2032.[64] The latter expansion in market size reflects annual growth rates estimated

between 12–16%,[64–67] driven primarily by rising demand in the automotive, energy, and consumer electronics industries, with the fastest growth rates in Asia-Pacific regions.[68,69] As these sectors continue to embrace supercapacitors for their rapid charge-discharge capabilities and reliability, the volume of end-of-life supercapacitors is expected to increase significantly along with market adoption. Effective recycling and re-purposing strategies will play a pivotal role in mitigating environmental impact and optimizing resource utilization.

The activated carbon market for supercapacitors is segmented by type into four categories based on surface area: under 1500 $m^2 g^{-1}$, 1500–1900 $m^2 g^{-1}$, 2000–2200 $m^2 g^{-1}$, and above 2200 $m^2 g^{-1}$. The segment under 1500 $m^2 g^{-1}$ leads the market,[65] which is also the type investigated in the current study (Table 2). This segmentation reflects the diverse applications and performance requirements across industries. However, precise industry-specific data on exact annual tonnages used remains undisclosed due to competitive reasons and proprietary formulations. As a general estimate, based on our specific device, we assume that activated carbon material constitutes approximately 10% of the device's total mass, equating to about 10 g in a typical 100 g device (*Supporting Information*, Table S2). This figure supports our hypothesis that activated carbon, even in relatively small amounts, has significant potential for recycling and re-purposing. For example, with minimal modification, such as NaOH etching, these 10 g of activated carbon could be re-purposed as electrodes for electrochemical desalination cells. Assuming a desalination cell with a lifetime of 200 cycles and a salt removal capacity of 6 mg g^{-1} per cycle (Figure 4B), this would translate to 12 g of NaCl removal in the supercapacitor's second life as a desalination cell, which would otherwise be disposed of.

Further advancements, as demonstrated by CO_2 treatment in this study (Figure 4E), can enhance both desalination capacity and stability, potentially increasing the salt removal capacity even further. Based on the specifications of a typical tube furnace, a maximum power of 1.5 kW is required for the heat treatment. Given the heating rate of 5 °C min^{-1} to reach 700 °C from room temperature, followed by 2 h holding time at 700 °C, a duration of 255 min furnace operation could be assumed, resulting in 4.25 kWh electrical energy consumption. The latter consumed electrical energy, which translates to a price of 1.70 € for each heat treatment trial, taking an average electricity price of 0.402 € per kWh in Germany in the second half of 2023 for household consumers (eurostat 04/2024). Going from laboratory-scale to industrial-scale practices, the latter price could further plummet when the mass of treated carbon in each heat treatment trial reaches kilogram levels. As such, we speculate that the benefits gained in terms of desalination capacity and stability by the CO_2 heat treatment of supercapacitor electrodes would outweigh the costs incurred because of heat treatment.

The re-purposing strategy not only extends the lifecycle of the materials but also contributes to reducing waste and promoting sustainability. The supercapacitors, known for their high specific power of approximately 10 kW kg^{-1},[70] generally have low specific energy contents. For instance, the energy content of the commercial supercapacitor used in this study is calculated to be only 0.625 Wh for a device weighing around 100 g (*Supporting Information*, Table S2). As such, future studies could explore re-purposing battery-type electrodes to achieve substantially higher desalination capacities. However, the latter approach presents specific challenges, particularly concerning electrode stability in aqueous media.

While traditional desalination technologies such as reverse osmosis (RO) are well-established, they require significant energy inputs, complex infrastructure, and often high operational costs.[71] A direct comparison between the performance metrics of RO and electrochemical desalination systems is often complicated by the non-equal salt rejection of the two. That is, RO systems have salt rejection rates of above 99%,[72] while it is much lower in electrochemical desalination systems (depending on the water recovery ratio; Ref.[73,74]). As such, a bypass stream from the feed to the product water is commonly considered in an RO setup to reduce its salt rejection rate close to that of an electrochemical desalination system.[75,76] Electrochemical desalination, mainly capacitive deionization, system becomes more energy efficient than RO for desalination of lower salinity regimes (brackish water), where NaCl concentration in the feedwater is lower than 2 g L^{-1} (or 34 mM).[75–78] The present study, which studies the capacitive deionization to desalinate NaCl solutions with 20 mM concentration, falls within the latter energy-efficient regime. Additionally, the re-purposing of end-of-life supercapacitors for electrochemical desalination presents a cost-effective solution by leveraging existing materials that would otherwise contribute to electronic waste.

Conclusions

The present work demonstrates the feasibility of re-purposing end-of-life commercial supercapacitors as electrochemical desalination systems, aligning with circular economy principles. By dissecting a commercial 500-Farad supercapacitor and extracting its electrodes, we investigated various modification methods, including NaOH-etching, CO_2 activation, and binder-added wet processing. We studied their performance for electrochemical water desalination applications. While the NaOH-etched electrodes showed an average desalination capacity of 5.8 mg g^{-1}, the CO_2-activated electrodes significantly improved desalination capacity (7.9 mg g^{-1}) and charge efficiency (above 90%) with stable performance over 20 cycles. These findings highlight a novel and practical approach to recycling supercapacitors, potentially reducing electronic waste and contributing to sustainable water desalination technologies. As such, this work opens new avenues for resource recovery and re-purposing, emphasizing the importance of resource management in achieving environmental sustainability.

Experimental Section

Supercapacitor Disassembly Process and Recovery of Material

Several HY-CAP 500 F 3 V supercapacitors were purchased from Reichelt Elektronik GmbH. The technical specifications of the latter commercial supercapacitor are listed in *Supporting Information*, Table S1. Figure S1 and Videos S1–2 in the *Supporting Information* demonstrate the step-by-step process of opening the commercial supercapacitor and recovering the electrodes. Typically, the electrode bundle is removed and unrolled after force-opening the aluminum casing of the commercial supercapacitor and discarding the small amount of electrolyte inside. The unrolled electrode consists of a white, non-woven separator paper covering a meter-long carbon-coated aluminum current collector. Scanning electron micrographs of the separator paper can be found in *Supporting Information*, Figure S2. After removing the separator, the carbon-coated aluminum current collector is dipped in 10 mass% NaOH solution using a tweezer. The carbon coating then easily peels off from the aluminum substrate after around 1 min, which is then washed with ample water and dried in a vacuum oven overnight at room temperature. The latter carbon electrode obtained is labeled herein as a NaOH-etched electrode. In the next step, the latter electrode is placed in a tube furnace (Carbolite Gero) at the rate of 5 °C min^{-1} under Ar atmosphere to reach 700 °C. Ar gas is then replaced by CO_2 at 700 °C for 2 h. At the end of 2 h, the CO_2 flow is again replaced with Ar while the furnace cools to the ambient temperature at 5 °C min^{-1}.

Electrode Preparation

To prepare counter electrodes for half-cell electrochemical testing, we followed the procedure described in our previous works to prepare free-standing carbon films.[55,79] Typically, the free-standing electrodes were fabricated by mixing activated carbon (type YP-80 F, Kuraray) with ethanol in an Agate mortar until the mixture was thoroughly wetted, using a pestle for manual stirring. Once a homogenous consistency was achieved, polytetrafluoroethylene binder (PTFE, 60 mass% dispersion in water from Sigma Aldrich) was added to serve as a polymeric binder, maintaining a carbon-to-binder mass ratio of 9 : 1. The stirring continued under a fume hood until the ethanol partially evaporated, resulting in a carbon paste. The latter paste was then cold rolled using a rolling machine (MTI HR01, MTI Corp.), resulting in free-standing carbon films with a thickness of ~600 μm. The films were gently placed on an aluminum foil and dried in a vacuum oven (Memmert) at +50 °C overnight. The latter resulted in carbon film electrodes with ~22 mg cm^{-2} mass loadings.

The NaOH-etched electrode material was blended with 5 mass% of PTFE binder and calendared with a rolling machine to reprocess supercapacitor electrodes. The resulting free-standing carbon films with a wet thickness of 600 μm were then dried in a vacuum oven at +50 °C overnight. Electrodes of 12 mm were punched for electrochemical characterization.

Electrochemical Half-Cell Measurements

We employed custom-built cells constructed from polyether ether ketone (PEEK) equipped with spring-loaded titanium pistons for electrochemical benchmarking in aqueous electrolytes.[80] These cells were configured in a three-electrode setup for electrochemical assessments. The electrode discs, each having a diameter of 12 mm (1.13 cm^2), were obtained by punching them out from electrode films. An Ag/AgCl electrode with 3 M KCl (E_0 Ag/AgCl = 0.210 V vs. normal hydrogen electrode) served as the reference electrode. A graphite current collector (0.25 mm thin foils, Sigraflex F02510TH, SGL Carbon) served as the current collector. Initially, a round piece of the latter graphite foil with a 12 mm diameter was punched and placed in the bottom of the cell. Then, a round-shaped working electrode with 12 mm diameter was placed onto the graphite current collector, followed by placing two vacuum-dried, 13 mm diameter, compressed glass-fiber separator disks (GF/A, 210 μm thickness, Whatman) to prevent short-circuiting. The counter electrode was punched into round-shaped films with a 12 mm diameter and positioned on top of the separator. Finally, another piece of graphite current collector was placed on top of the latter. Two titanium pistons are loaded with springs to sandwich the cell components together. The electrolyte was an aqueous 600 mM NaCl filled into the cell by vacuum backfilling. The Ag/AgCl reference electrode was positioned on top of a glass fiber separator in a cavity designed in the cell to be close to the sandwiched stack of working and counter electrodes.

The electrochemical performance testing included cyclic voltammetry (CV) and electrochemical impedance spectroscopy (EIS), utilizing a VMP3 multi-channel potentiostat/galvanostat from Bio-Logic with the EC-Lab software. CV was conducted to ascertain the electrochemical behavior and stability window of the system, employing a scan rate of 1 mV s^{-1}, commencing at 0 V vs. Ag/AgCl to a potential of +1.0 V/−1.0 V vs. Ag/AgCl in steps of 0.1 V. EIS measurements was carried out at open circuit potential (OCP), +0.6 V vs. Ag/AgCl and −0.8 V vs. Ag/AgCl with a sinusoidal signal of 5 mV in the frequency range from 100 kHz to 1 mHz. The commercial supercapacitor underwent galvanostatic charge and discharge with a cell voltage of 2.8 V at 1 A current with a Bio-Logic battery cycler. All electrochemical measurements were performed in a climate chamber (Binder) where the temperature was constant at +25 ± 1 °C.

To determine the electrochemical stability region of the electrolyte, the S-values for the positive and negative polarizations were calculated following Equation (1) and Equation (2), respectively:[51]

$$S_{pos} = \frac{Q_+}{Q_-} - 1 \tag{1}$$

$$S_{neg} = \frac{Q_-}{Q_+} - 1 \tag{2}$$

where Q_+ and Q_- are the integrated charges during the anodic and cathodic scans, respectively.

Electrochemical Desalination

The electrochemical desalination tests were performed following the best practice methods we recently reported.[81] A symmetric cell with a pair of electrodes (extracted from the supercapacitor) was fabricated. An electrochemical workstation (Bio-Logic VSP300) was programmed to charge and discharge the cell repeatedly at 0.1 A g^{-1} based on the combined average mass of both carbon electrodes. A 10 L tank containing 20 mM aqueous NaCl electrolyte was constantly flushed with nitrogen gas to remove dissolved oxygen. The 20 mM NaCl concentration was chosen to mimic the brackish water salinity levels[40,81] and as a concentration regime where electrochemical desalination is more energy-efficient than conventional desalination technologies such as reverse osmosis.[75–78]

A peristaltic pump (Masterflex) continuously circulated the latter electrolyte to the cell at 2 mL min^{-1}, which was subsequently passed through a chamber housing a conductivity meter (Met-

rohm). The conductivity was then related to the concentration using the calibration equation that measured several NaCl stock solutions in the 1 mM to 50 mM aqueous NaCl concentration range. The desalination capacity (DC) is then calculated following Equation (3).

$$DC = \frac{\nu\, M}{60\, m_{total}} \int C\, dt \tag{3}$$

where ν is the flow rate (mL min^{-1}), M is the molar mass of the NaCl (58.44 g mol^{-1}), m_{total} is the total mass of both electrodes combined (mg), t is the time (s) during which a concentration change (mM) occurs, and DC (mg g^{-1}) is the amount of salt (mg) taken up per gram of the electrodes. The charge efficiency (CE) of the system is calculated according to Equation (4).

$$CE = \frac{DC\, F\, m_{total}}{1000\, q\, M} \times 100\% \tag{4}$$

where F is the Faraday constant (96485 C mol^{-1}), and q is the electronic charge (mA s) stored in the electrodes.

The energy consumption of the system is calculated according to Equation (5).

$$\text{Energy consumption} = \frac{\frac{U_{charge}}{m_{total}}}{\frac{DC}{M_{NaCl}}} \tag{5}$$

Where the (U_{charge}) is the energy consumed during the charging, m_{total} is the total mass of both electrodes, DC is obtained from Equation (3) and 58.44 g mol^{-1} for the molar mass of NaCl (M_{NaCl}).

Material Characterizations

X-ray diffraction (XRD) analysis was conducted using a D8 Advance diffractometer (Bruker AXS) equipped with a copper X-ray source (Cu–Kα, λ = 1.5406 Å, 40 kV, 40 mA). The samples were analyzed over the 3.5° to 80° 2θ range at 0.033 s per step. Before analysis, the dry powder was pressed onto an optical glass sample holder featuring a 0.5 mm deep notch for sample preparation. Scanning electron microscopy (SEM) images were captured using a ZEISS GEMINI 500 field-emission scanning electron microscope with 0.5–1 kV acceleration voltage. Energy-dispersive X-ray (EDX) spectroscopy was conducted at 15 kV utilizing an X–Max Silicon Detector from Oxford Instruments with the AZtec software. Sample preparation involved mounting them on an aluminum stub using double-sided copper tape without an additional sputtering step. At least 20 random points were selected on each sample for point elemental analysis, with subsequent calculation of the average quantities of the detected elements.

Nitrogen adsorption at −196 °C was carried out using an Autosorb iQ system (Quantachrome, now Anton Paar). Before analysis, samples underwent degassing at 200 °C for 12 h. Specific surface area (SSA) calculations were conducted using Brunauer-Emmett-Teller (BET) theory alongside quenched-solid density functional theory (QSDFT), assuming a slit-shaped pore model. Raman spectroscopic analysis was conducted using a Renishaw inVia Raman microscope featuring a Nd:YAG laser (532 nm). Laser power at the sample's focal point was rigorously maintained at 0.05 mW, with a numerical aperture of 0.75. Spectra were recorded at five distinct points for each sample, with an exposure time of 30 s per point and measurements accumulated five times to bolster reliability. The to-be-analyzed powder samples were firmly pressed onto glass slides to ensure stability. Spectra underwent meticulous processing for cosmic ray removal and subsequent normalization to ensure consistency (0–1). System calibration with a silicon standard was rigorously performed before and after the measurements to uphold accuracy. Thermogravimetric analysis (TGA) was performed using a Netzsch TG-209–1 Libra. Mass changes up to 900 °C were recorded at a heating rate of 5 °C min^{-1} in an oxidative atmosphere (synthetic air) with argon as a protective gas. Further runs were conducted using pure argon and CO_2 atmosphere.

Supporting Information Summary

Supporting information is available online, which includes: Two videos showing the disassembly process of the commercial supercapacitor and unrolling of the electrode bundle, a summary of gas sorption results (Table S1), specifications of the commercial supercapacitor (Table S2), a comparison with other electrochemical desalination works (Table S3), pictures of the step-by-step disassembly process of the supercapacitor (Figure S1), SEM images of supercapacitor separator (Figure S2) and active materials (Figure S3), nitrogen gas sorption analysis of the electrodes (Figure S4), nitrogen gas sorption isotherms of the CO_2-activated electrodes (Figure S5), plots of potential stability limits (Figure S6), cyclic voltammetry measurement of CO_2-activated electrodes (Figure S7), picture of the soldered commercial supercapacitor (Figure S8), electrochemical characterization of the commercial supercapacitor (Figure S9), pictures of the supercapacitor with holes for direct re-purposing as electrochemical desalination cell (Figure S10), and electrochemical desalination performance of an additional CO_2-activated electrode (Figure S11).

Author Contributions

Panyu Ren: Investigation, Data curation, Visualization, Writing – Original Draft, Writing – Review & Editing. **Mohammad Torkamanzadeh**: Investigation, Data curation, Visualization, Supervision, Writing – Original Draft, Writing – Review & Editing. **Stefanie Arnold**: Investigation, Data curation, Visualization, Supervision, Writing – Original Draft, Writing – Review & Editing. **Emmanuel Pameté**: Methodology, Investigation, Data curation, Writing – Original Draft, Writing – Review & Editing. **Volker Presser**: Conceptualization, Supervision, Validation, Resources, Visualization, Writing – Original Draft, Writing – Review & Editing, Project administration, Funding acquisition.

Acknowledgements

The authors acknowledge Dr. Gracita Raquel Tomboc, Dr. Behnoosh Bornamehr, and Dr. Tamara Winter (all at INM, present or past) for their kind support in conducting various tests for us. E.P. acknowledges funding from the Alexander von Humboldt Foundation. V.P. and E.P. acknowledge funding of the joint Polish-German project SUPILMIX (PR-1173/27) by the

German Research Foundation (DFG, Deutsche Forschungsgemeinschaft) and the Polish National Science Centre (NCN, National Science Centre). Open Access funding enabled and organized by Projekt DEAL.

Conflict of Interests

The authors declare no conflict of interest.

Data Availability Statement

The data that support the findings of this study are available from the corresponding author upon request.

Keywords: Carbon · Electrochemistry · Recycling · Supercapacitor · Water desalination

[1] A. K. Awasthi, V. R. S. Cheela, I. D'Adamo, E. Iacovidou, M. R. Islam, M. Johnson, T. R. Miller, K. Parajuly, A. Parchomenko, L. Radhakrishan, M. Zhao, C. Zhang, J. Li, *Resources, Environment and Sustainability* **2021**, *3*, 100014.
[2] S. Sundriyal, V. Shrivastav, H. D. Pham, S. Mishra, A. Deep, D. P. Dubal, *Resour., Conserv. Recycl.* **2021**, *169*, 105548.
[3] Y. Wang, Y. Zhang, L. Pei, D. Ying, X. Xu, L. Zhao, J. Jia, X. Cao, *Sci. Rep.* **2017**, *7*, 41523.
[4] Y. Yang, S. Mao, Z. Li, Z. Sun, R. Zhao, *Water Sci. Technol.* **2021**, *84*, 1011–1022.
[5] L. Minzae, K. Gil-Pyo, S. Hyeon Don, P. Soomin, Y. Jongheop, *Nanotechnol.* **2014**, *25*, 345601.
[6] Y. Wang, M. Jiang, Y. Yang, F. Ran, *Electrochim. Acta* **2016**, *222*, 1914–1921.
[7] J. Sreńscek-Nazzal, J. Serafin, A. Kamińska, A. Dymerska, E. Mijowska, B. Michalkiewicz, *J. Colloid Interface Sci.* **2022**, *627*, 978–991.
[8] M. M. Vadiyar, X. Liu, Z. Ye, *ChemSusChem* **2018**, *11*, 2410–2420.
[9] J. H. Rademaker, R. Kleijn, Y. Yang, *Environ. Sci. Technol.* **2013**, *47*, 10129–10136.
[10] K. Baba, Y. Hiroshige, T. Nemoto, *Hitachi Rev.* **2013**, *62*, 452–455.
[11] S. Högberg, T. S. Pedersen, F. B. Bendixen, N. Mijatovic, B. B. Jensen, J. Holboll, *Direct reuse of rare earth permanent magnets – Wind turbine generator case study, 2016 XXII International Conference on Electrical Machines (ICEM)*, IEEE, **2016**, 1625–1629, https://ieeexplore.ieee.org/abstract/document/7732741.
[12] J. Zhu, I. Mathews, D. Ren, W. Li, D. Cogswell, B. Xing, T. Sedlatschek, S. N. R. Kantareddy, M. Yi, T. Gao, Y. Xia, Q. Zhou, T. Wierzbicki, M. Z. Bazant, *Cell Rep. Phys. Sci.* **2021**, *2*, 100537.
[13] J. Thakur, C. Martins Leite de Almeida, A. G. Baskar, *J. Cleaner Prod.* **2022**, *375*, 134066.
[14] Y. Li, S. Arnold, S. Husmann, V. Presser, *J. Energy Storage* **2023**, *60*, 106625.
[15] J. Wu, M. Zheng, T. Liu, Y. Wang, Y. Liu, J. Nai, L. Zhang, S. Zhang, X. Tao, *Energy Storage Mater.* **2023**, *54*, 120–134.
[16] L. Zhang, Z. Xu, Z. He, *ACS Sustain. Chem. Eng.* **2020**, *8*, 11596–11605.
[17] J. Zhang, M. Gu, X. Chen, *Micro and Nano Eng.* **2023**, *21*, 100229.
[18] F. Béguin, V. Presser, A. Balducci, E. Frackowiak, *Adv. Mater.* **2014**, *26*, 2219–2251.
[19] J. Zhao, A. F. Burke, *J. Energy Chem.* **2021**, *59*, 276–291.
[20] P. Saha, S. Dey, M. Khanra, *J. Power Sources* **2021**, *496*, 229824.
[21] S. Zhang, N. Pan, *Adv. Energy Mater.* **2015**, *5*, 1401401.
[22] R. Chaari, O. Briat, J. Y. Delétage, E. Woirgard, J. M. Vinassa, *Microelectron. Reliab.* **2011**, *51*, 1976–1979.
[23] E. Pameté, L. Köps, F. A. Kreth, S. Pohlmann, A. Varzi, T. Brousse, A. Balducci, V. Presser, *Adv. Energy Mater.* **2023**, *13*, 2301008.
[24] H. Trivedi, K.D. Verma, K.K. Kar, *Recycling of Supercapacitor Materials, Handbook of Nanocomposite Supercapacitor Materials IV: Next-Generation Supercapacitors*, Springer **2023**, 331, 393-411, https://link.springer.com/chapter/10.1007/978-3-031-23701-0_16.
[25] J. Mao, C. Ye, S. Zhang, F. Xie, R. Zeng, K. Davey, Z. Guo, S. Qiao, *Energy Environ. Sci.* **2022**, *15*, 2732–2752.
[26] Z. J. Baum, R. E. Bird, X. Yu, J. Ma, *ACS Energy Lett.* **2022**, *7*, 712–719.
[27] X. Wang, G. Gaustad, C. W. Babbitt, *Waste Manage.* **2016**, *51*, 204–213.
[28] X. Qu, B. Zhang, J. Zhao, B. Qiu, X. Chen, F. Zhou, X. Li, S. Gao, D. Wang, H. Yin, *Green Chem.* **2023**, *25*, 2992–3015.
[29] X. Qu, M. Cai, B. Zhang, H. Xie, L. Guo, D. Wang, H. Yin, *Green Chem.* **2021**, *23*, 8673–8684.
[30] E. Gratz, Q. Sa, D. Apelian, Y. Wang, *J. Power Sources* **2014**, *262*, 255–262.
[31] G. Jiang, S. J. Pickering, *Waste Manage.* **2016**, *48*, 465–470.
[32] A. Dutta, J. Mahanta, T. Banerjee, *Adv. Sustainable Syst.* **2020**, *4*, 2000182.
[33] N. R. Chodankar, S. J. Patil, S.-K. Hwang, P. A. Shinde, S. V. Karekar, G. S. R. Raju, K. S. Ranjith, A. G. Olabi, D. P. Dubal, Y. S. Huh, Y.-K. Han, *Energy Storage Materials.* **2022**, *49*, 564–574.
[34] F. Wu, T. Zhao, Y. Yao, T. Jiang, B. Wang, M. Wang, *Chemosphere* **2020**, *238*, 124638.
[35] J. Choi, P. Dorji, H. K. Shon, S. Hong, *Desalination* **2019**, *449*, 118–130.
[36] S. Lei, T. Yang, C. Tian, T. Yan, X. Li, W. Song, W. Liu, L. Yan, Y. Zhao, *Desalination* **2024**, *574*, 117248.
[37] S. Porada, R. Zhao, A. van der Wal, V. Presser, P. M. Biesheuvel, *Prog. Mater. Sci.* **2013**, *58*, 1388–1442.
[38] S.-J. Seo, H. Jeon, J. K. Lee, G.-Y. Kim, D. Park, H. Nojima, J. Lee, S.-H. Moon, *Water Res.* **2010**, *44*, 2267–2275.
[39] L. Wang, S. Lin, *Environ. Sci. Technol.* **2019**, *53*, 5797–5804.
[40] L. Huang, T. Yan, A. E. D. Mahmoud, S. Li, J. Zhang, L. Shi, D. Zhang, *Environ. Sci.: Nano* **2021**, *8*, 950–959.
[41] G. Wang, T. Yan, J. Shen, J. Zhang, L. Shi, D. Zhang, *Environ. Sci.: Nano.* **2021**, *8*, 122–130.
[42] M. Mao, T. Yan, J. Shen, J. Zhang, D. Zhang, *Environ. Sci. Technol.* **2021**, *55*, 3333–3340.
[43] L. Wang, L. Deligniere, S. Husmann, R. Leiner, C. Bahr, S. Zhang, C. Dun, M. M. Montemore, M. Gallei, J. J. Urban, C. Kim, V. Presser, *Nano Res.* **2023**, *16*, 9352–9363.
[44] A. Jänes, H. Kurig, E. Lust, *Carbon* **2007**, *45*, 1226–1233.
[45] R. P. Vidano, D. B. Fischbach, L. J. Willis, T. M. Loehr, *Solid State Commun.* **1981**, *39*, 341–344.
[46] Y. Zheng, R. Zhang, P. Vanaphuti, J. Fu, Z. Yang, Y. Wang, *ACS Sustainable Chem. Eng.* **2021**, *9*, 6087–6096.
[47] L. A. Gomez-Moreno, A. Klemettinen, R. Serna-Guerrero, *iScience* **2023**, *26*, 107782.
[48] K. S. W. Sing, D. H. Everett, R. A. W. Haul, L. Moscou, R. A. Pierotti, J. Rouquerol, T. Siemieniewska, *Pure Appl Chem.* **1985**, *57*, 603–619.
[49] Q. Gao, L. Demarconnay, E. Raymundo-Pinero, F. Beguin, *Energy Environ. Sci.* **2012**, *5*, 9611–9617.
[50] E. Pameté, F. Beguin, *Electrochim. Acta* **2021**, *389*, 138687.
[51] D. Weingarth, H. Noh, A. Foelske-Schmitz, A. Wokaun, R. Kotz, *Electrochim. Acta* **2013**, *103*, 119–124.
[52] S. Porada, L. Borchardt, M. Oschatz, M. Bryjak, J. S. Atchison, K. J. Keesman, S. Kaskel, P. M. Biesheuvel, V. Presser, *Energy Environ. Sci.* **2013**, *6*, 3700–3712.
[53] C. Kim, P. Srimuk, J. Lee, S. Fleischmann, M. Aslan, V. Presser, *Carbon* **2017**, *122*, 329–335.
[54] B. Krüner, P. Srimuk, S. Fleischmann, M. Zeiger, A. Schreiber, M. Asian, A. Quade, V. Presser, *Carbon* **2017**, *117*, 46–54.
[55] M. Aslan, M. Zeiger, N. Jäckel, I. Grobelsek, D. Weingarth, V. Presser, *J. Phys.: Condens. Matter* **2016**, *28*, 114003.
[56] N. Jäckel, M. Rodner, A. Schreiber, J. Jeongwook, M. Zeiger, M. Aslan, D. Weingarth, V. Presser, *J. Power Sources* **2016**, *326*, 660–671.
[57] T. Kim, J. Yoon, *RSC Adv.* **2015**, *5*, 1456–1461.
[58] P. Ren, M. Torkamanzadeh, X. Zhang, M. Twardoch, C. Kim, V. Presser, *Carbon* **2023**, *213*, 118191.
[59] A. P. Silva, A. Argondizo, P. T. Juchen, L. A. M. Ruotolo, *Sep. Purif. Technol.* **2021**, *271*, 118872.
[60] J. Kim, Y. Yi, D.-H. Peck, S.-H. Yoon, D.-H. Jung, H. S. Park, *Environ. Sci.: Nano* **2019**, *6*, 916–924.
[61] Z. Xie, X. Shang, J. Yan, T. Hussain, P. Nie, J. Liu, *Electrochim. Acta* **2018**, *290*, 666–675.
[62] M. Kim, H. Lim, X. Xu, M. S. A. Hossain, J. Na, N. N. Awaludin, J. Shah, L. K. Shrestha, K. Ariga, A. K. Nanjundan, D. J. Martin, J. G. Shapter, Y. Yamauchi, *Microporous and Mesoporous Mater.* **2021**, *312*, 110757.
[63] M. E. Suss, S. Porada, X. Sun, P. M. Biesheuvel, J. Yoon, V. Presser, *Energy Environ. Sci.* **2015**, *8*, 2296–2319.

[64] Precedence Research, Supercapacitors market size, share, and trends 2024 to 2034, **2024**, https://www.precedenceresearch.com/supercapacitors-market.
[65] Precedence Research, Supercapacitor activated carbon market report overview, **2024**, https://www.businessresearchinsights.com/market-reports/supercapacitor-activated-carbon-market-104798.
[66] MarketsandMarkets Research, Supercapacitor market by type (double layer capacitors, pseudocapacitors, hybrid capacitors), electrode material (carbon, metal oxide, conducting polymers, composites)application (automotive, energy, consumer electronics- Global Forecast to 2027, 2024, https://www.marketsandmarkets.com/Market-Reports/supercapacitor-market-37140453.html.
[67] https://www.transparencymarketresearch.com/supercapacitor-market.htmlMarketsandMarkets Research, Supercapacitor Market, 2024, https://www.transparencymarketresearch.com/supercapacitor-market.htmlhttps://www.marketsandmarkets.com/Market-Reports/supercapacitor-market-37140453.html.
[68] S. Ghosh, S. Yadav, A. Devi, T. Thomas, *Renewable Sustainable Energy Rev.* **2022**, *161*, 112412.
[69] Y. Yang, Y. Han, W. Jiang, Y. Zhang, Y. Xu, A.M. Ahmed, *Applied Sciences* **2021**, *12*, 354.
[70] S. M. Benoy, M. Pandey, D. Bhattacharjya, B. K. Saikia, *J. Energy Storage* **2022**, *52*, 104938.
[71] M. Qasim, M. Badrelzaman, N. N. Darwish, N. A. Darwish, N. Hilal, *Desalination* **2019**, *459*, 59–104.
[72] C. Bartels, R. Franks, S. Rybar, M. Schierach, M. Wilf, *Desalination* **2005**, *184*, 185–195.
[73] S. Porada, L. Zhang, J. E. Dykstra, *Desalination* **2020**, *488*, 114383.
[74] H. K. Mutha, H. J. Cho, M. Hashempour, B. L. Wardle, C. V. Thompson, E. N. Wang, *Desalination* **2018**, *437*, 154–163.
[75] M. Qin, A. Deshmukh, R. Epsztein, S. K. Patel, O. M. Owoseni, W. S. Walker, M. Elimelech, *Desalination* **2019**, *455*, 100–114.
[76] P. Sharan, T. J. Yoon, S. M. Jaffe, T. Ju, R. P. Currier, A. T. Findikoglu, *Cleaner Eng. Technol.* **2021**, *3*, 100102.
[77] X. Liu, S. Shanbhag, T. V. Bartholomew, J. F. Whitacre, M. S. Mauter, *ACS ES&T Eng.* **2021**, *1*, 261–273.
[78] S.-Y. Pan, A. Z. Haddad, A. Kumar, S.-W. Wang, *Water Res.* **2020**, *183*, 116064.
[79] M. Torkamanzadeh, L. Wang, Y. Zhang, O. Budak, P. Srimuk, V. Presser, *ACS App. Mater. Interfaces* **2020**, *12*, 26013–26025.
[80] D. Weingarth, M. Zeiger, N. Jäckel, M. Aslan, G. Feng, V. Presser, *Adv. Energy Mater.* **2014**, *4*, 1400316.
[81] M. Torkamanzadeh, C. Kök, P. R. Burger, P. Ren, Y. Zhang, J. Lee, C. Kim, V. Presser, *Cell Rep. Phys. Sci.* **2023**, *4*, 101661.

Manuscript received: July 28, 2024
Revised manuscript received: August 26, 2024
Accepted manuscript online: August 27, 2024
Version of record online: October 23, 2024